Structural Engineering and Mechanics, *Vol. 56, No. 2 (2015) 293-315*
DOI: http://dx.doi.org/10.12989/sem.2015.56.2.293

Influence of wind disturbance on smart stiffness identification of building structure using limited micro-tremor observation

Ryuji Koyama, Kohei Fujita and Izuru Takewaki*

Department of Architecture and Architectural Engineering, Kyoto University, Nishikyo, Kyoto 615-8540, Japan

(Received January 29, 2015, Revised September 8, 2015, Accepted October 19, 2015)

Abstract. While most of researches on system identification of building structures are aimed at finding modal parameters first and identifying the corresponding physical parameters by using the transformation in terms of transfer functions and cross spectra, etc., direct physical parameter system identification methods have been proposed recently. Due to the problem of signal/noise (SN) ratios, the previous methods are restricted mostly to earthquake records or forced vibration data. In this paper, a theoretical investigation is performed on the influence of wind disturbances on stiffness identification of building structures using micro-tremor at limited floors. It is concluded that the influence of wind disturbances on stiffness identification of building structures using micro-tremor at limited floors is restricted in case of using time-series data for low-rise buildings and does not cause serious problems.

Keywords: system identification; micro-tremor; wind disturbance; physical parameter; limited observation

1. Introduction

The research on system identification of building structures has been progressed recently in response to the need of the development of techniques for damage detection (Agbabian *et al*. 1991, Yao and Natke 1994, Doebling *et al*. 1996, Masri *et al*. 1996, Barroso and Rodriguez 2004, Nagarajaiah and Basu 2009, Hernandez-Garcia *et al*. 2010, Ji *et al*. 2011, Kuwabara *et al*. 2013) and structural health monitoring in order to manage the business continuity plan and upgrade the earthquake resilience of building structures (Hart and Yao 1977, Safak 1989, Ghanem and Shinozuka 1995, Hjelmstad *et al*. 1995, Lus *et al*. 2004, Housner *et al*. 1997, Takewaki *et al*. 2011). Most of researches are aimed at finding modal parameters first and identifying the corresponding physical parameters by using the transformation in terms of transfer functions and cross spectra, etc. (see Fig. 1(a)). While this approach seems to be reliable and stable, the appropriateness of employed models (shear building model, shear-bending model, frame model) is closely related to the accuracy of the identification of physical parameters (Minami *et al*. 2013).

On the other hand, some methods have been developed which identify the physical parameters directly from a set of earthquake records at limited floors. Udwadia *et al*. (1978) proposed a theory on system identification of shear buildings using earthquake records at the upper and lower floors

*Corresponding author, Professor, E-mail: takewaki@archi.kyoto-u.ac.jp

http://www.techno-press.org/?journal=sem&subpage=8 ISSN: 1225-4568 (Print), 1598-6217 (Online)

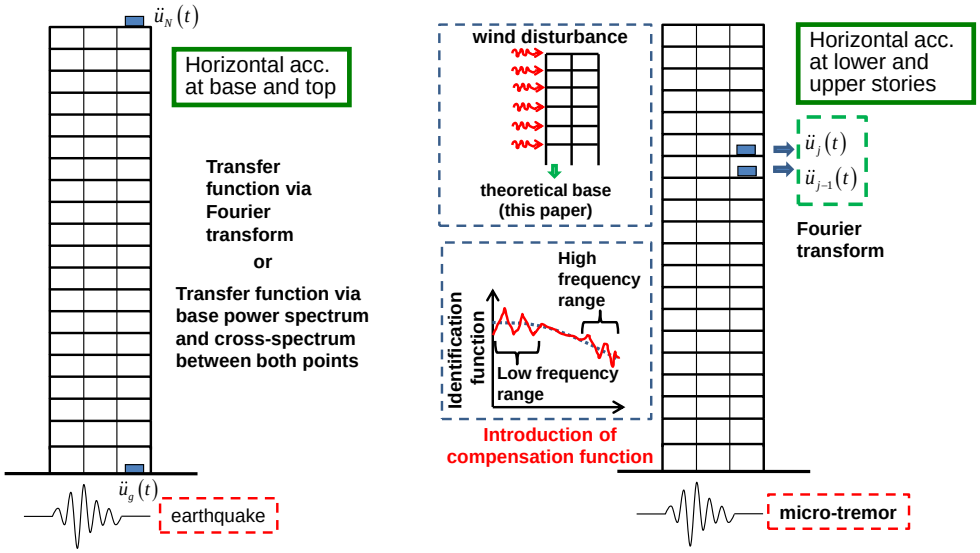

(a) Conventional method (b) Proposed method

Fig. 1 Conventional method and proposed method with compensation algorithm

of the object story. Takewaki and Nakamura (2000) reformulated the method in terms of Fourier transforms and showed that the damping can also be identified by using the zero-frequency limit (see Fig. 1(b)). They also showed that the proposed method can work well in actual situations. The method has been extended to a shear-bending model and the ARX (Auto Regressive eXogenous) model has been introduced to overcome the difficulty arising from noise issues (Takewaki and Nakamura 2005, 2009, Kuwabara *et al*. 2013, Minami *et al*. 2013, Ikeda *et al*. 2014a).

Some other methods have also been proposed for identifying the story stiffnesses or damages of shear building models by using an iterative method (Zhang and Johnson 2012, 2013a, b, Johnson and Wojtkiewicz 2014, Mei and GülNovel 2014). However its applicability to actual buildings has never been presented.

Due to the problem of signal/noise (SN) ratios, the previous methods are restricted mostly to earthquake records or forced vibration data. However, earthquake records and forced vibration data are difficult to obtain in a timely manner. In this situation, it is believed that the micro-tremor is suitable (Ikeda *et al*. 2014b). In dealing with micro-tremors, the problems of SN ratios and influence of external disturbances, e.g. wind loading, have to be resolved. It is well known theoretically that the cross spectra between the base and building roof can remove the noise due to wind loading. However the applicability of such technique to the direct physical parameter system identification may not be clear.

The purpose of this paper is to theoretically investigate the influence of wind loading on stiffness identification of building structures using micro-tremors at limited floors. It is concluded that the influence of wind loading on stiffness identification of building structures using micro-tremors at limited floors is restricted to a lower frequency range for rather low-rise buildings in which the response of the building structure is not employed in the identification because of the small power of responses derived from the time-series data resulting from the nonexistence of eigenvibrations in that region.

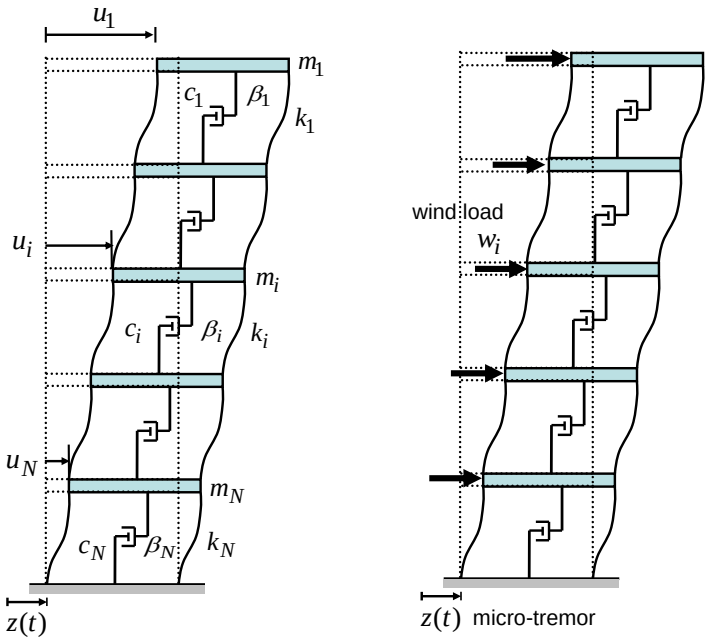

(a) Shear building model (b) Shear building model under micro-tremor and wind load

Fig. 2 Shear building model under micro-tremor and wind disturbance

2. Stiffness identification of shear buildings under micro-tremor and wind loading using limited observation

2.1 Governing equation

Consider an *N*-story shear building model, as shown in Fig. 2(a), with viscous and material dampings (Nashif *et al*. 1985, Inaudi and Kelly 1995) in parallel. Although material damping is not used afterward, it is included here to make the formulation general. Numbering of the nodes and elements is made from the top. This is because this numbering enables the smooth connection with the previous formulation and makes the manipulation systematic. The *j*th node and the *j*th element from the top are called the "node *j*" and the "element *j*", respectively. Let m_j and k_j denote the mass of the node *j* and the story stiffness of the element *j*. Let c_j and β_j be the viscous damping coefficient and the material damping ratio in the element *j*. The complex stiffness of the element *j* is described as $k_j^* = k_j(1+2\beta_j i)$ where *i* is the imaginary unit.

This shear building model is subjected both to the horizontal base acceleration $\ddot{z}(t)$ as a micro-tremor and wind loading $\mathbf{w}(t)=\{w_1...w_j...w_N\}^T$ (w_j: horizontal wind loading at node *j*) as shown in Fig. 2(b). $(\ )^T$ denotes the vector transpose. The equations of motion of this model in the frequency domain may be expressed as

$$\left(-\omega^2\mathbf{M}+i\omega\mathbf{C}+\mathbf{K}\right)\mathbf{U}(\omega)=\mathbf{F}(\omega)Z(\omega)+\mathbf{W}(\omega) \tag{1}$$

where $\mathbf{U}(\omega)$, $Z(\omega)$ and $\mathbf{W}(\omega)$ are the Fourier transforms of the absolute horizontal nodal

displacements $\mathbf{u}(t)$, the base displacement $z(t)$ and wind loading $\mathbf{w}(t)$, respectively. The mass, stiffness and damping matrices $\mathbf{M}$, $\mathbf{K}$, $\mathbf{C}$ and the vectors $\mathbf{W}(\omega)$, $\mathbf{F}(\omega)$ are defined by

$$\mathbf{M} = diag\begin{pmatrix} m_1 & m_2 & \cdots & m_N \end{pmatrix} \tag{2}$$

$$\mathbf{K} = \begin{bmatrix} k_1^* & -k_1^* & & \\ -k_1^* & k_1^* + k_2^* & -k_2^* & \\ & & \ddots & \\ & & -k_{N-1}^* & k_{N-1}^* + k_N^* \end{bmatrix} \tag{3}$$

$$\mathbf{C} = \begin{bmatrix} c_1 & -c_1 & & \\ -c_1 & c_1 + c_2 & -c_2 & \\ & & \ddots & \\ & & -c_{N-1} & c_{N-1} + c_N \end{bmatrix} \tag{4}$$

$$\mathbf{W}(\omega) = \begin{Bmatrix} W_1 & W_2 & \cdots & W_N \end{Bmatrix}^T \tag{5}$$

$$\mathbf{F}(\omega) = \begin{Bmatrix} 0 & 0 & \cdots & i\omega c_N + k_N^* \end{Bmatrix}^T \tag{6}$$

Eq. (1) can be expressed in a compact form as

$$\mathbf{A}(\omega)\mathbf{U}(\omega) = \mathbf{R}(\omega)Z(\omega) \tag{7}$$

where

$$\mathbf{A}(\omega) = \begin{bmatrix} a_1(\omega) & -b_1(\omega) & & \\ -b_1(\omega) & a_2(\omega) & \ddots & \\ & \ddots & \ddots & -b_{N-1}(\omega) \\ & & -b_{N-1}(\omega) & a_N(\omega) \end{bmatrix} \tag{8}$$

$$\mathbf{R}(\omega) = \begin{Bmatrix} (W_1/Z) & (W_2/Z) & \cdots & (W_N/Z) + i\omega c_N + k_N^* \end{Bmatrix}^T \tag{9}$$

In Eq. (8), $a_j(\omega)$ and $b_j(\omega)$ can be expressed as

$$\begin{aligned} a_j(\omega) &= -\omega^2 m_j + i\omega c_{j-1} + k_{j-1}^* + i\omega c_j + k_j^* \\ &= -\omega^2 m_j + b_{j-1}(\omega) + b_j(\omega) \end{aligned} \tag{10}$$

$$b_j(\omega) = i\omega c_j + k_j^* \tag{11}$$

The vector $\mathbf{R}(\omega)$ in Eq. (9) related to wind loading can be expressed as follows.

$$\begin{aligned}\mathbf{R}(\omega) &= \left\{ D_1 \quad D_2 \quad \cdots \quad D_N + i\omega c_N + k_N^* \right\}^T \\ &= \left\{ R_1 \quad R_2 \quad \cdots \quad R_N \right\}^T\end{aligned} \tag{12}$$

where

$$D_i = \frac{W_i}{Z} \tag{13}$$

For the necessity in a later formulation, the frequency-domain wind loading at node i is assumed to have the following property.

$$W_i = (i\omega)^2 W_{\mathrm{co}}^i + O(\omega^3) \tag{14}$$

where W_{co}^i is the coefficient. In this case, the following relation is satisfied.

$$\lim_{\omega \to 0} (d^2 W_i / d\omega^2) = -2W_{\mathrm{co}}^i \tag{15}$$

The constraint (14) indicates that the frequency-domain wind loading has zero value and zero first-order sensitivity at zero frequency. This property corresponds to the across-wind direction loading. This condition is used in Eqs. (39) and (47) later. Since the across-wind direction loading has a zero-mean property, the zero static (frequency=0) term may be acceptable. It is also true that the property around zero frequency of the Fourier spectrum of the across-wind direction loading has not been made clear even experimentally (Balendra 1993). Based on this fact, the assumption of Eq. (14) seems acceptable. Furthermore, since the power of micro-tremor and its influence are small in a lower frequency range, the constraint (14) does not seem to cause a serious problem for the reliability and stability of the proposed identification theory.

2.2 Identification of Nth-story stiffness

Let us derive $U_j(\omega)$ in this section. By conducting the mathematical manipulation, $\mathbf{U}(\omega)$ can be derived from Eq. (7).

$$\mathbf{U}(\omega) = \frac{adj(\mathbf{A})}{\det(\mathbf{A})} \mathbf{R}(\omega) Z(\omega) \tag{16}$$

where $adj(\mathbf{A})$ is the adjugate matrix (transpose of the cofactor matrix) of $\mathbf{A}$. After the introduction of definition of $adj(\mathbf{A})$, Eq. (16) leads to

$$U_j(\omega) = \sum_{l=1}^{N} \left\{ (-1)^{l+j} \frac{\det(\mathbf{A}_{lj})}{\det(\mathbf{A})} R_l \right\} Z \tag{17}$$

where $\mathbf{A}_{lj}$ is the matrix deleting the lth row and the jth column.

Let Δ_j denote the determinant of the matrix replacing the jth column of the matrix $\mathbf{A}$ with $\mathbf{R}$. In case of $j=N$, Δ_N can be expressed as

$$\Delta_N = \det \begin{bmatrix} a_1 & -b_1 & & & & R_1 \\ -b_1 & a_2 & -b_2 & & & R_2 \\ & \ddots & \ddots & \ddots & & \vdots \\ & & -b_{N-3} & a_{N-2} & -b_{N-2} & R_{N-2} \\ & & & -b_{N-2} & a_{N-1} & R_{N-1} \\ & & & & -b_{N-1} & R_N \end{bmatrix} \tag{18}$$

Cofactor expansion at the jth column of the determinant of the matrix replacing the jth column of the matrix $\mathbf{A}$ with $\mathbf{R}$ provides

$$\Delta_j = \sum_{l=1}^{N} \left\{ (-1)^{l+j} \det\left(\mathbf{A}_{jl}\right) R_l \right\} \tag{19}$$

Due to the symmetry of $\mathbf{A}$, the following relation holds.

$$\det\left(\mathbf{A}_{jl}\right) = \det\left(\mathbf{A}_{lj}\right) \tag{20}$$

Eqs. (17), (19) and (20) yield the frequency-domain displacement at node j.

$$U_j = \frac{\Delta_j}{P_N} Z \tag{21}$$

where $P_j(\omega)$ is the determinant of the principal minor of $j \times j$ from the left top of $\mathbf{A}$ (P_0=1, P_N=det $\mathbf{A}$). Substitution of Eq. (18) into Δ_j in Eq. (21) and the relation between R_i and D_i in Eq. (12) lead to

$$\frac{U_N}{Z} = b_N \frac{P_{N-1}}{P_N} + \sum_{l=1}^{N} \left\{ (-1)^{l+N} D_l \frac{\det\left(\mathbf{A}_{lN}\right)}{P_N} \right\} \tag{22}$$

Eq. (22) corresponds to Eq. (12) in the reference (Takewaki and Nakamura 2000) and includes the effect of wind loading expressed by $\{D_j\}$.

Cofactor expansion of det $\mathbf{A}_{N\text{-}1N}$ at (N-1)th row provides

$$\det\left(\mathbf{A}_{N-1\ N}\right) = (-1)^{N+N-1}\left(-b_{N-1}\right) P_{N-2} \tag{23}$$

Substitution of Eq. (23) into Eq. (22) and expansion of the summation procedure lead to

$$\frac{U_N}{Z} = \left(b_N + D_N\right)\frac{P_{N-1}}{P_N} + b_{N-1}D_{N-1}\frac{P_{N-2}}{P_N} + \cdots + \left(b_1 b_2 \cdots b_{N-1}\right) D_1 \frac{P_0}{P_N} \tag{24}$$

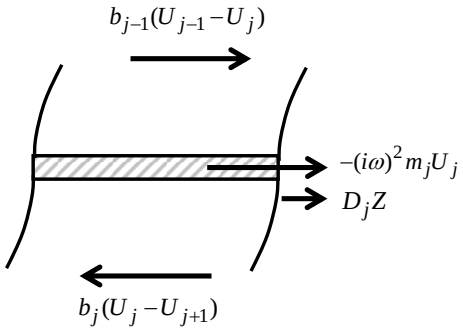

Fig. 3 Dynamic equilibrium at node *j*

Let us define the quantity $Q_j(\omega)$ which represents the Fourier transform of the story shear force in the element *j* by multiplying $-\mathrm{i}\omega U_{j+1}(\omega)$ (Takewaki and Nakamura 2000). From the internal equilibrium, the following relation holds.

$$b_j\left(U_j-U_{j+1}\right)=-i\omega U_{j+1}Q_j \tag{25a}$$

Substitution of $j=N$ into Eq. (25a) leads to

$$b_N\left(U_N-U_{N+1}\right)=-i\omega U_{N+1}Q_N \tag{25b}$$

Dividing both sides of Eq. (25b) by $U_{N+1}(=Z)$, the following relation can be drawn.

$$Q_N=\frac{b_N}{i\omega}\left(1-\frac{U_N}{Z}\right) \tag{25c}$$

Substituting Eq. (22) into Eq. (25c), Q_N can be derived as follows.

$$Q_N=\frac{b_N}{i\omega}\left\{1-b_N\frac{P_{N-1}}{P_N}-\sum_{l=1}^{N}\left(\left(-1\right)^{l+N}D_l\frac{\det\left(\mathbf{A}_{lN}\right)}{P_N}\right)\right\} \tag{26}$$

Eq. (25) and the dynamic equilibrium at node *j* (see Fig. 3) provide

$$-i\omega U_{j+1}Q_j=-i\omega U_jQ_{j-1}-\left(i\omega\right)^2 m_jU_j+D_jZ \tag{27}$$

where D_j is defined in Eq. (13). Division of both sides of Eq. (25) by $i\omega U_j$ and multiplication by Q_j on the resulting equation yield

$$Q_j=\frac{\dfrac{b_j}{i\omega}\dfrac{U_{j+1}}{U_j}Q_j}{\dfrac{b_j}{i\omega}+\dfrac{U_{j+1}}{U_j}Q_j} \tag{28}$$

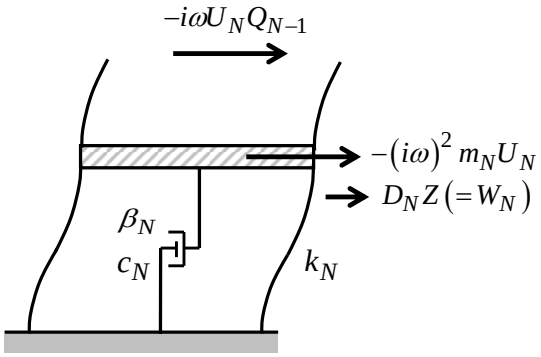

Fig. 4 Relation among story shear $-i\omega U_N Q_{N-1}$, inertial force $-(i\omega)^2 m_N U_N$ and wind load $D_N Z(=W_N)$

Eqs. (27) and (28) lead to the expression of Q_j in terms of Q_{j-1}.

$$Q_j = \frac{b_j}{i\omega} \frac{Q_{j-1} + i\omega m_j - \dfrac{D_j Z}{i\omega U_j}}{\dfrac{b_j}{i\omega} + Q_{j-1} + i\omega m_j - \dfrac{D_j Z}{i\omega U_j}} \tag{29}$$

Eq. (29) corresponds to Eq. (8) in the reference (Takewaki and Nakamura 2000) and includes the effect of wind loading expressed by $\{D_j\}$. Substitution of Eq. (29) in case of $j=N$ into Q_N in Eq. (26) provides

$$b_N \frac{P_{N-1}}{P_N} = 1 - \sum_{l=1}^{N} \left\{ (-1)^{l+N} D_l \frac{\det(\mathbf{A}_{lN})}{P_N} \right\} - \frac{Q_{N-1} + i\omega m_N - \dfrac{D_N Z}{i\omega U_N}}{\dfrac{b_N}{i\omega} + Q_{N-1} + i\omega m_N - \dfrac{D_N Z}{i\omega U_N}} \tag{30}$$

Deletion of $b_N(P_{N-1}/P_N)$ from Eq. (30) using Eq. (22) leads to

$$\frac{U_N}{Z} = \frac{b_N}{i\omega} \frac{1}{i\omega m_N + \dfrac{b_N}{i\omega} + Q_{N-1} - \dfrac{D_N Z}{i\omega U_N}} \tag{31}$$

Slight modification of Eq. (31) yields

$$\frac{(i\omega)^2 U_N}{Z - U_N} = \frac{b_N}{m_N + \dfrac{Q_{N-1}}{i\omega} - \dfrac{D_N Z}{(i\omega)^2 U_N}} \tag{32}$$

Eq. (32) corresponds to Eq. (19) in the reference (Takewaki and Nakamura 2000) and includes the effect of wind loading expressed by $\{D_j\}$. In fact, the denominator of the right-hand side of Eq. (32) multiplied by $(i\omega)^2 U_N$ consists of three parts, i.e., inertial force of node N, story shear force

of (*N*-1)th element and wind load at node *N*. This is illustrated in Fig. 4.

In the previous stiffness identification theory (Takewaki and Nakamura 2000) using the identification function, the limit manipulation $\omega \to 0$ is necessary in the expression of the left-hand side of Eq. (32). For this reason, the limit manipulation is considered in the denominator of the right-hand side of Eq. (32). The following relation holds.

$$\lim_{\omega \to 0} \left\{ m_N + \frac{Q_{N-1}}{i\omega} - \frac{D_N Z}{(i\omega)^2 U_N} \right\} = m_N + \lim_{\omega \to 0} \left\{ \frac{Q_{N-1}}{i\omega} \right\} - \lim_{\omega \to 0} \left\{ \frac{D_N Z}{(i\omega)^2 U_N} \right\} \tag{33}$$

From Eq. (26) the second term in Eq. (33) can be expressed as follows.

$$\lim_{\omega \to 0} \left(\frac{Q_{N-1}}{i\omega} \right) = \lim_{\omega \to 0} \left(\frac{b_{N-1}}{(i\omega)^2} \right) \left\{ \lim_{\omega \to 0} \left(1 - b_{N-1} \frac{P_{N-2}}{P_{N-1}} \right) - \lim_{\omega \to 0} \left(D_{\text{sum}}^{N-1} \right) \right\} \tag{34}$$

where D_{sum}^{N-1} is expressed as

$$D_{\text{sum}}^{N-1} = D_{N-1} \frac{P_{N-2}}{P_{N-1}} + b_{N-2} D_{N-2} \frac{P_{N-3}}{P_{N-1}} + \cdots + (b_1 b_2 \cdots b_{N-2}) D_1 \frac{P_0}{P_{N-1}} \tag{35}$$

Let us expand $P_j(\omega)$ at $\omega \to 0$.

$$\lim_{\omega \to 0} P_j(\omega) = \lim_{\omega \to 0} (b_1 b_2 \cdots b_j) \tag{36}$$

Substitution of Eq. (36) into Eq. (35) leads to the limit value of $b_{N-1} D_{\text{sum}}^{N-1}$.

$$\lim_{\omega \to 0} \left(b_{N-1} D_{\text{sum}}^{N-1} \right) = \lim_{\omega \to 0} \left(D_{N-1} + D_{N-2} + \cdots + D_1 \right) \tag{37}$$

Substitution of Eq. (36) into Eq. (34) yields

$$\lim_{\omega \to 0} \left\{ \frac{b_{N-1}}{(i\omega)^2} \left(1 - b_{N-1} \frac{P_{N-2}}{P_{N-1}} \right) \right\} = m_1 + m_2 + \cdots m_{N-1} \tag{38}$$

The wind loading W_i in Eq. (14) can be re-expressed as

$$D_i = \frac{W_{\text{co}}^i}{Z} (i\omega)^2 + O(\omega^3) \tag{39}$$

The second term in the second parenthesis in Eq. (34) can be reduced to the following form using Eqs. (37) and (39).

$$\lim_{\omega \to 0} \left(\frac{b_{N-1}}{(i\omega)^2} D_{\text{sum}}^{N-1} \right) = \frac{W_{\text{co}}^1}{\lim_{\omega \to 0} Z} + \frac{W_{\text{co}}^2}{\lim_{\omega \to 0} Z} + \cdots + \frac{W_{\text{co}}^{N-1}}{\lim_{\omega \to 0} Z} \tag{40}$$

$\lim_{\omega\to 0} Z \neq 0$ is assumed here.

Furthermore, from the property of the transfer function, the following relation holds.

$$\lim_{\omega\to 0}\left(\frac{Z}{U_N}\right)=1 \tag{41a}$$

Substitution of Eqs. (39) and (41a) into the third term in Eq. (33) provides

$$\lim_{\omega\to 0}\left\{\frac{D_N Z}{(i\omega)^2 U_N}\right\}=\frac{W_{\mathrm{co}}^N}{\lim_{\omega\to 0} Z} \tag{41b}$$

These expressions will be used in the following.

The equation for identifying the story stiffness of a shear building model under micro-tremor and wind loading is shown next.

Substitution of Eqs. (33), (38), (40) and (41b) into Eq. (32) provides

$$\mathrm{Re}\left\{\lim_{\omega\to 0}\left(\frac{(i\omega)^2 U_N}{Z-U_N}\right)\right\}=\mathrm{Re}\left\{\lim_{\omega\to 0}\left(\frac{b_N}{\sum_{l=1}^{N} m_l - W_{\mathrm{sum}}^N}\right)\right\} \tag{42}$$

where

$$W_{\mathrm{sum}}^N=\frac{W_{\mathrm{co}}^1}{\lim_{\omega\to 0} Z}+\frac{W_{\mathrm{co}}^2}{\lim_{\omega\to 0} Z}+\cdots+\frac{W_{\mathrm{co}}^N}{\lim_{\omega\to 0} Z} \tag{43}$$

Define $G(\omega)$ by Eq. (44) in view of Eq. (42).

$$\mathrm{Re}\left\{\lim_{\omega\to 0} G(\omega)\right\}=\mathrm{Re}\left[\lim_{\omega\to 0}\left\{\frac{(i\omega)^2 U_N}{Z-U_N}\left(\sum_{l=1}^{N} m_l - W_{\mathrm{sum}}^N\right)\right\}\right]=k_N \tag{44}$$

It can be observed that the real part of the limit of $G(\omega)$ at $\omega\to 0$ provides the story stiffness k_N. W_{sum}^N indicates the sum of wind loads at all the nodes as shown in Fig. 5.

3. Accuracy and reliability investigation of proposed method using frequency-domain simulation

3.1 Comparison of floor response under micro-tremor with actual floor response

The comparison of simulated floor responses under actual micro-tremor without wind loading with actual floor responses is shown in this section for investigating the influence of wind loading on floor responses under micro-tremor.

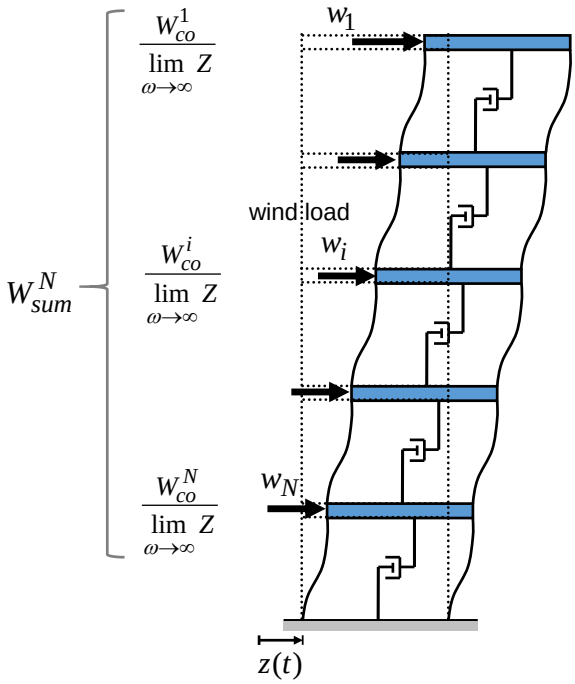

Fig. 5 Meaning of compensation term W_{sum}^{N}

Fig. 6 Five-story steel building and installed velocity meter (Ikeda *et al*. 2014b)

The micro-tremor at the base measured in a 5-story steel building at Uji Campus of Kyoto University in 2013 is used as input here (see Figs. 6 and 7). Measured velocity data are transformed into acceleration data. Those velocity and acceleration data are shown in Figs. 8 and 9. Fig. 10 shows a simulated top-floor response under this micro-tremor without wind loading with the corresponding actual floor response. It can be observed that the influence of wind loading is significant under micro-tremor.

3.2 Accuracy investigation of proposed identification method using frequency-domain simulation

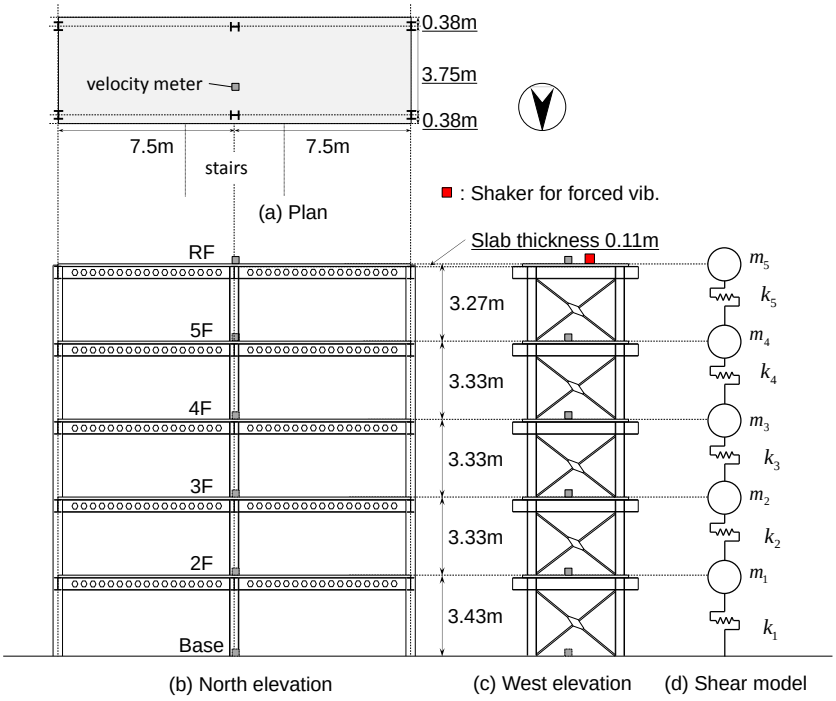

Fig. 7 Frame dimension and its shear building model (Ikeda *et al*. 2014b)

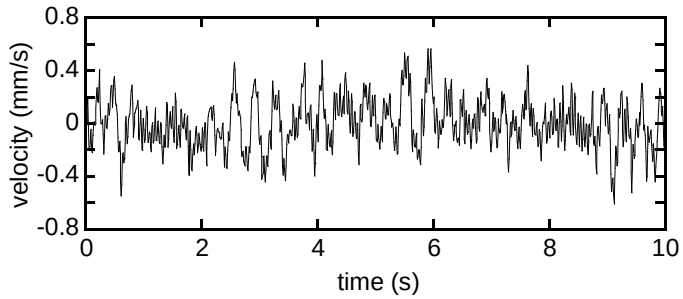

Fig. 8 Ground velocity as micro-tremor

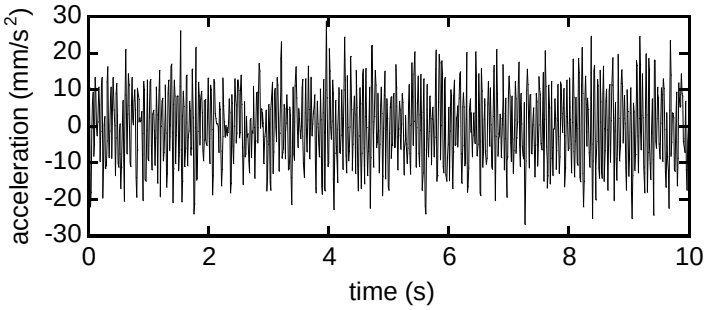

Fig. 9 Ground acceleration evaluated from velocity

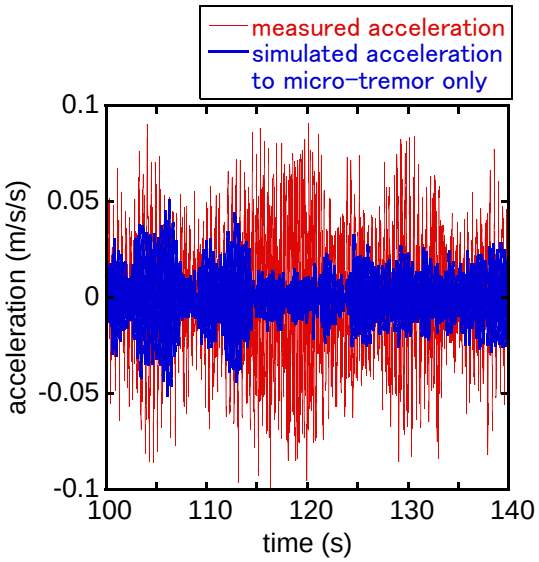

Fig. 10 Roof acceleration (measured one and simulated one to micro-tremor only)

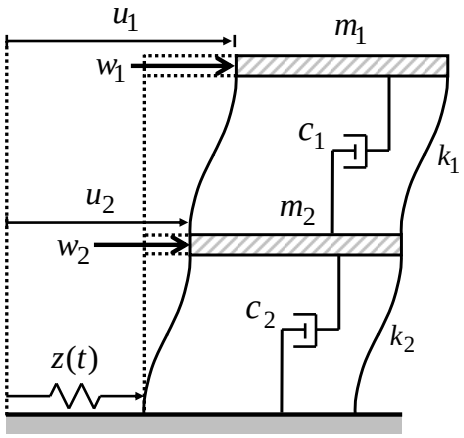

Fig. 11 Two-story shear building model under micro-tremor and wind load

The validity of the theory for micro-tremor and wind loading developed in Section 2 is investigated here. The frequency-domain simulation is used in this section.

Consider a two-story shear building model as shown in Fig. 11. The model parameters are shown in Table 1. The fundamental and second natural circular frequencies are 24.2 and 63.5 (rad/s). The input micro-tremor is the measured one in a 5-story steel building at Uji Campus of Kyoto University stated above. The same band-limited white noise is used as simulated wind loadings at two floor levels. In the proposed method, ground micro-tremor is used and the corresponding wind disturbance is not the strong wind, but the weak wind. It is well known that, while the strong wind exhibits a peculiar character, the weak wind possesses a rather random character. Such random character may be well represented by white-noise-like inputs. A band-limited white noise with null around zero frequency satisfying the constraint (14) is used in

Table 1 Parameters of 2-story shear building model

	Mass ($\times 10^4$ kg)	Story stiffness ($\times 10^4$ kN/m)	Damping coefficient ($\times 10^2$ kN·s/m)
First story	2.6	4.0	5.0
Second story	2.6	4.0	5.0

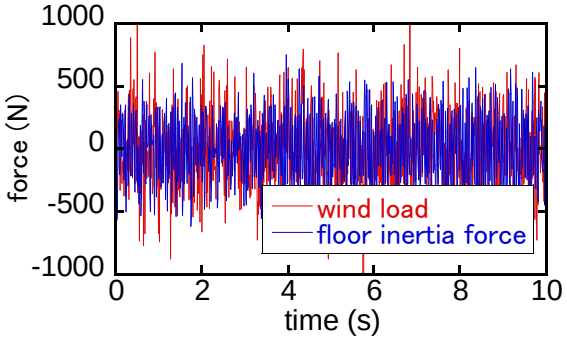

Fig. 12 Floor inertia force and wind load

the actual numerical simulation.

The level of band-limited white noise with null around zero frequency is scaled so as to be approximately equivalent to the inertia forces (floor mass×base acceleration due to micro-tremor). The standard deviation of the band-limited white noise as wind loading is 300(N). The inertia force and the wind load are shown in Fig. 12.

3.3 Identification equation for story stiffness

The floor displacement response in the frequency domain can be expressed as

$$\begin{Bmatrix} U_1 \\ U_2 \end{Bmatrix} = \mathbf{A}^{-1} \begin{pmatrix} R_1 \\ R_2 \end{pmatrix} Z \tag{45}$$

Rearrange the second component of Eq. (45) as

$$\frac{U_2}{Z} = \frac{b_1 R_1 + a_1 R_2}{a_1 a_2 - b_1 b_1} \tag{46}$$

In Eq. (44), it has been shown that the real part of the limit of $G(\omega)$ at $\omega \to 0$ provides the story stiffness k_N. In order to investigate in detail the property of $G(\omega)$, the following function is defined.

$$E(\omega) = \mathrm{Re}\left\{ \frac{(i\omega)^2 U_N}{Z - U_N} \left(\sum_{l=1}^{N} m_l - \bar{W}_{\mathrm{sum}}^{N}(\omega) \right) \right\} \tag{47}$$

where $\lim_{\omega \to 0} \{E(\omega)\} = k_N$ and $\bar{W}_{\mathrm{sum}}^{N}(\omega)$ is defined by

$$\bar{W}_{\text{sum}}^{N}(\omega)=\bar{W}_1(\omega)+\bar{W}_2(\omega)+\cdots+\bar{W}_N(\omega) \tag{48}$$

In Eq. (48), $\bar{W}_i(\omega)$ indicates

$$\bar{W}_i(\omega)=\frac{W_i(\omega)}{(i\omega)^2 Z(\omega)} \tag{49}$$

Eq. (47) represents the *'modified identification function for micro-tremor and wind loading'*.

It is possible to evaluate the story stiffness from the limit value of Eq. (47) in the case of the input of micro-tremor and wind loading. On the other hand, the function for the case without wind loading can be expressed as

$$E_{\text{ori}}(\omega)=\text{Re}\left(\frac{(i\omega)^2 U_N}{Z-U_N}\sum_{l=1}^{N} m_l\right) \tag{50}$$

It can be understood that the original case without wind loading can be obtained by substituting $\bar{W}_{\text{sum}}^{N}(\omega)=0$ in Eq. (47).

3.4 Comparison between characteristic functions E(ω) and E_{ori}(ω) for wind loading of various levels

The comparison is shown here between the characteristic functions $E(\omega)$ and $E_{ori}(\omega)$ for wind loading of various levels larger than the inertia forces. $E(\omega)$ and $E_{ori}(\omega)$ are shown in Figs. 13 and 14. The simulated frequency-domain floor response data for the case under micro-tremor and wind loading have been used for evaluating $E(\omega)$ and $E_{ori}(\omega)$. The standard deviation of the wind loads has been changed from 500 (n) to 5000 (N) which is larger than the inertia force.

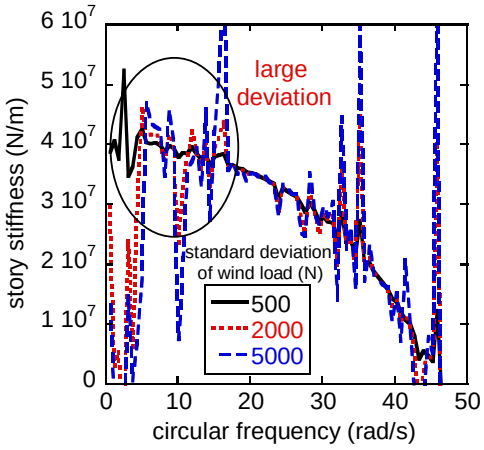

Fig. 13 Story stiffness identification under wind loading of various levels larger than inertia force using $E_{ori}(\omega)$

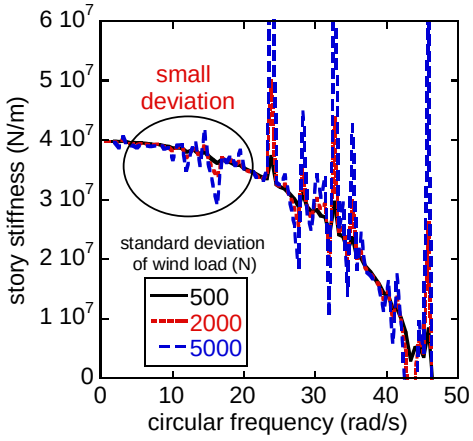

Fig. 14 Story stiffness identification under wind loading of various levels larger than inertia force using $E(\omega)$

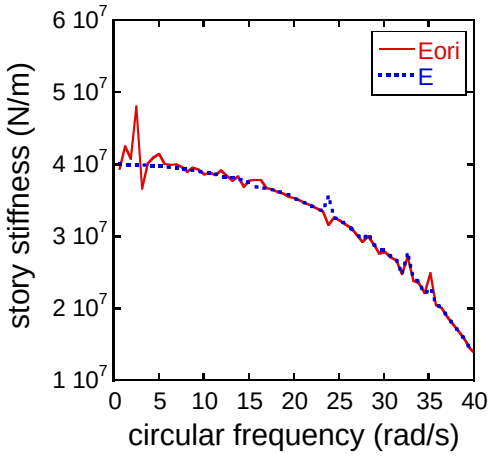

Fig. 15 Story stiffness identification under wind loading of level equivalent to inertia force using $E(\omega)$ and $E_{ori}(\omega)$

It can be observed from Fig. 13, since the influence of wind loading is not reflected in Eq. (50), the function $E_{ori}(\omega)$ deviates greatly especially in a lower frequency range. On the other hand, it is seen from Fig. 14, because the influence of wind loading is reflected appropriately in Eq. (47), the deviation of the function $E(\omega)$ in a lower frequency range is small and converges to the theoretical value 4.0×10^4 kN/m at $\omega\rightarrow0$.

It can be concluded that the function $E(\omega)$ and the corresponding proposed theory in Section 2 and Section 3 enable one to identify the story stiffness reliably even under wind loading in the identification for micro-tremor input.

The comparison between the characteristic functions $E(\omega)$ and $E_{ori}(\omega)$ for wind loading of the level equivalent to inertia forces is shown here. As in Section 3.4, the simulated frequency-domain floor response data for the case under micro-tremor and wind loading have been used for evaluating $E(\omega)$ and $E_{ori}(\omega)$. Fig. 15 shows $E(\omega)$ and $E_{ori}(\omega)$ for the simulated frequency-domain floor response data. It can be observed that $E(\omega)$ exhibits a stable property and even $E_{ori}(\omega)$ shows

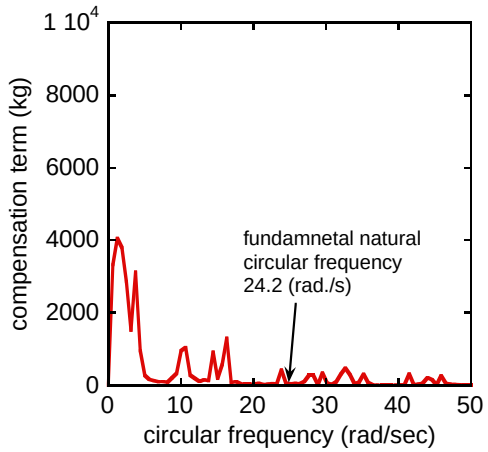

Fig. 16 Absolute value of $\bar{W}^2_{\text{sum}}(\omega)$

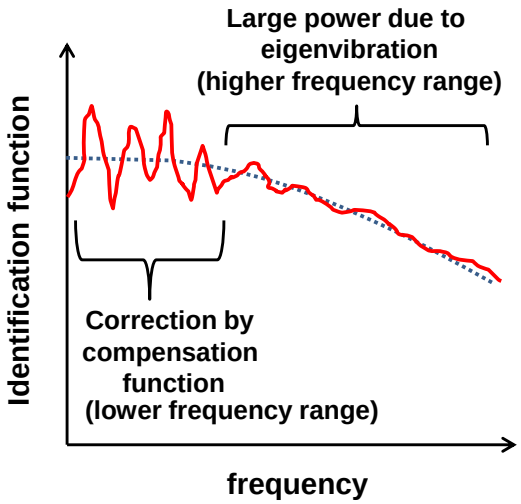

Fig. 17 Role of compensation function in correction of contaminated identification function

a relatively stable property. Furthermore the small deviation of $E_{ori}(\omega)$ is restricted to a lower frequency range. This reason will be investigated next.

The absolute value of the compensation term $\bar{W}^2_{\text{sum}}(\omega)$ in Eq. (47) is shown in Fig. 16. It can be seen that the absolute value of $\bar{W}^2_{\text{sum}}(\omega)$ is very small compared to the corresponding mass 5.2×10^4 kg especially in a higher frequency range. For this reason, even if the level of wind loading is almost equivalent to the level of inertia forces, the influence of wind loading is restricted to a lower frequency range. This supports the effectiveness of the proposed identification theory including Eq. (47) under micro-tremor and wind loading.

Fig. 17 illustrates the role of the proposed compensation function in the correction of contaminated identification functions. The contamination in the lower frequency range is removed by the compensation function. Furthermore the present identification function has a large power in

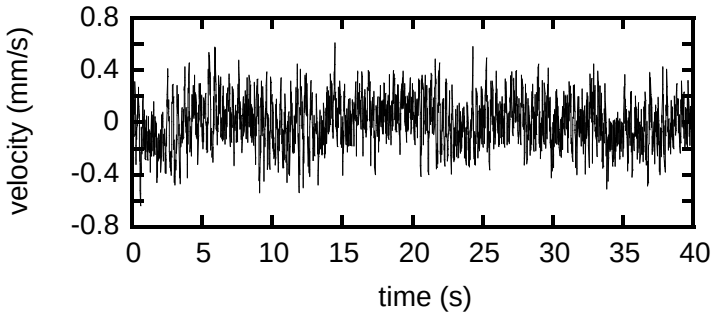

Fig. 18 Ground velocity as micro-tremor (duration=40s)

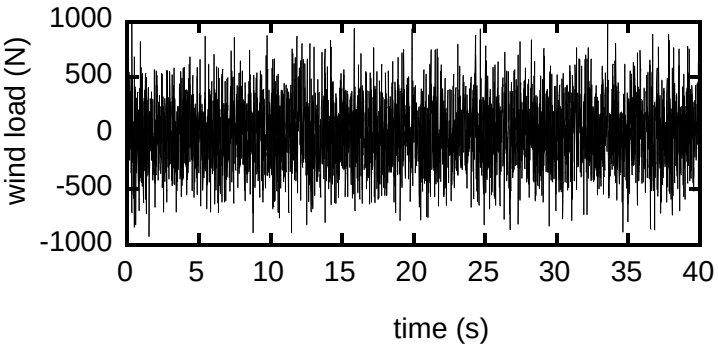

Fig. 19 Wind load (standard deviation=300N)

a higher frequency range due to the existence of eigenvibration in that frequency range.

A compensation term $\bar{W}_{\text{sum}}^{N}(\omega)$ has been introduced in order to show that the effect of wind loading on the accuracy of stiffness identification is not significant. Therefore it is unnecessary to compute the compensation term $\bar{W}_{\text{sum}}^{N}(\omega)$ in the actual identification of story stiffness via the proposed identification method.

4. Accuracy and reliability investigation of proposed method using time-domain simulation

4.1 Simulation model

The time-domain simulation is performed in this section. The two-story shear building model as shown in Fig. 11 (parameters shown in Table 1) is subjected to the micro tremor as shown in Fig. 18. The wind loading as a band-limited white noise (standard deviation is 300 N) with the level equivalent to inertia forces is considered. The wind load is shown in Fig. 19.

The time-history response analysis has been conducted by using the Newmark-beta method. The time-history displacement data have been Fourier transformed and substituted into Eqs. (47) and (50).

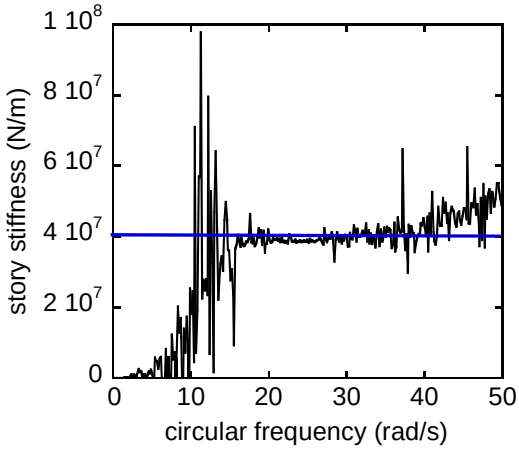

Fig. 20 Evaluation of first-story stiffness from $E(\omega)$ ($=E_{ori}(\omega)$) without wind loading

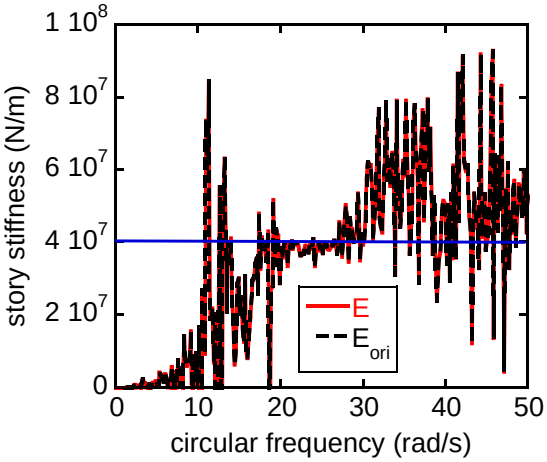

Fig. 21 Evaluation of first-story stiffness from $E(\omega)$ and $E_{ori}(\omega)$ with wind loading

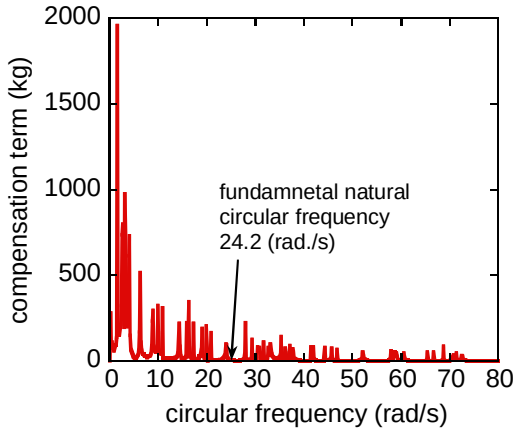

Fig. 22 Compensation term $\bar{W}_{\text{sum}}^2(\omega)$ for wind loading

4.2 Identification of story stiffness without wind loading

The function $E(\omega)$ ($=E_{ori}(\omega)$) for the first story without wind loading is shown in Fig. 20. The theoretical value is 4.0×10^4 kN/m. It can be observed that, when the wind loading does not exist, the stiffness can be evaluated approximately by using the previous method. However the power in a lower frequency range is small due to the property of micro-tremor. This is a remarkable difference between the frequency-domain simulation (Section 3) and the simulation using the time-series data (actual situation).

4.3 Identification of story stiffness with wind loading

The functions $E(\omega)$ and $E_{ori}(\omega)$ for the first story with wind loading are shown in Fig. 21. The absolute value of the compensation term $\bar{W}^2_{\text{sum}}(\omega)$ is shown in Fig. 22 and is quite small compared to the corresponding mass 5.2×10^4 kg especially in a higher frequency range. This figure corresponds with Fig. 16 obtained by the frequency-domain simulation. It can be concluded that the influence of wind loading on the stiffness identification is restricted to the lower frequency range due to the property of micro-tremor and the frequency characteristic of the proposed identification method, i.e., the frequency characteristic of the characteristic functions $E(\omega)$ and $E_{ori}(\omega)$ derived from the time-series data. Since the time-series data are used in the actual situation, this characteristic plays an important role. For this reason, it may be said that the proposed stiffness identification method has reliability even under wind loading. However the present discussion may apply to rather low-rise buildings with a high fundamental natural frequency. The investigation for middle-rise and high-rise buildings should be made in the future.

4.4 Identification result of story stiffness from previous research

For additional information, Ikeda *et al*. (2014b) used the same micro-tremor data measured in the 5-story steel building at Uji Campus in Kyoto University as stated in Section 3.1 (see Figs. 6 and 7) and identified the story stiffness by using the method employing the identification function, the ARX model and filtering techniques.

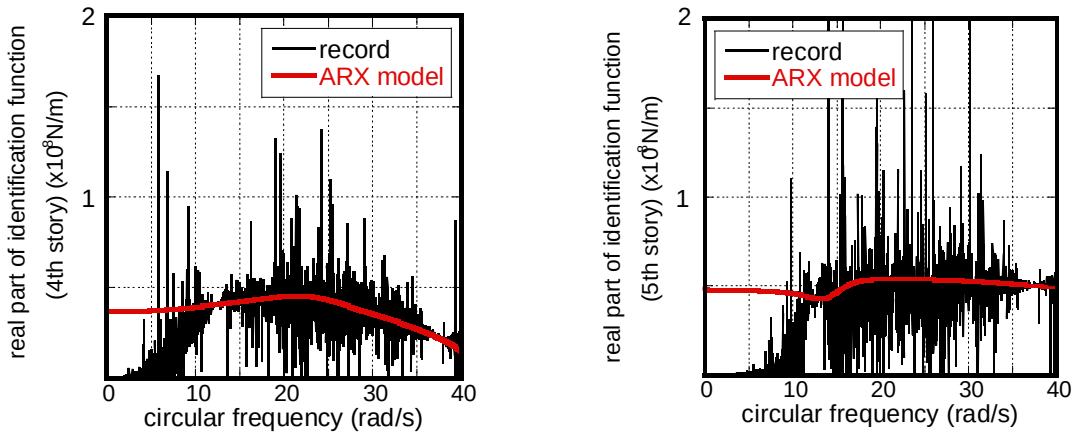

Fig. 23 Examples of real part of identification function (4th and 5th stories) (Ikeda *et al.* 2014b)

Table 2 Identified story stiffnesses via previous method (long-span direction) (Ikeda *et al*. 2014b)

		Preliminary static analysis	Identified value
story stiffness $\times 10^4$ (kN/m)	1st story	5.12	6.038
	2nd story	4.55	5.402
	3rd story	4.51	4.912
	4th story	4.47	4.612
	5th story	4.44	4.424

Fig. 23 shows two examples of the real part of identification functions (4th and 5th stories) (Ikeda *et al*. 2014b). The identification function, Eq. (50), without the compensation function has been used. It is found that, although some deviations are observed in the identification function after filtering only (black line), an acceptable identification may be possible after the further application of the ARX model (red line). This may result from the property of the method using the identification function and the fact that the influence of wind disturbances is restricted to a lower frequency range (see Figs. 16 and 22). On the other hand, in a higher frequency range where a large power exists due to the existence of eigenvibrations of the building, the ARX model and filtering enable the stabilization of the identification function. However, the determination of the ARX order and filtering parameters requires cumbersome tasks. It is expected that the stabilizing property shown in Figs. 13 and 14 further supports the reliable identification using the identification function even under wind disturbances.

Table 2 shows the mean value of the identified stiffnesses using the method proposed in the reference (Ikeda *et al*. 2014b). The result by the preliminary static analysis has also been presented for comparison.

5. Conclusions

(1) The inclusion of the effect of wind loading on direct stiffness identification of building structures is possible by imposing a constraint on the property of wind loading. The constraint indicates that the frequency-domain wind loading has zero value and zero first-order sensitivity at zero frequency. This property corresponds to the across-wind direction loading.

(2) The effect of wind loading on direct stiffness identification of building structures can be expressed by a ‘compensation function’ which indicates the difference from the identification function without wind loading.

(3) The validity of the present theory has been confirmed by the frequency-domain and time-domain simulations.

(4) The influence of wind loading on stiffness identification of building structures using micro-tremor at limited floors is restricted to a lower frequency range in which the response of the building structure is not employed in the identification because of the small power of responses in time-series data resulting from the nonexistence of eigenvibrations in that region.

(5) The facts stated in (1)-(4) may apply to rather low-rise buildings with a high fundamental natural frequency. The investigation for middle-rise and high-rise buildings should be made in the future. In that case, a shear-bending model should be introduced. The identification of bending stiffness may be a difficult issue in that model (Minami *et al*. 2013, Fujita *et al*. 2015).

Acknowledgments

Part of the present work is supported by the Grant-in-Aid for Scientific Research of Japan Society for the Promotion of Science (No. 24246095, 15H04079). This support is greatly appreciated. The authors are grateful to Miss A. Ikeda of Kyoto University for providing the analysis result for actual micro-tremor inputs.

References

Agbabian, M.S., Masri, S.F., Miller, R.K. and Caughey, T.K. (1991), "System identification approach to detection of structural changes", *J. Eng. Mech.*, ASCE, **117**(2), 370-390.

Balendra, T. (1993), *Vibration of Buildings to Wind and Earthquake Loads*, Springer-Verlag, London.

Barroso L.R. and Rodriguez, R. (2004), "Damage detection utilizing the damage index method to a benchmark structure", *J. Eng. Mech*., ASCE, **130**(2), 142-151.

Doebling S.W., Farrar, C.R., Prime, M.B. and Shevitz, D.W. (1996), "Damage identification and health monitoring of structural and mechanical systems from changes in their vibration characteristics: A literature review", Los Alamos National Laboratory Report LA-13070-MS.

Fujita, K., Ikeda, A., Shirono, M. and Takewaki, I. (2015), "System identification of high-rise buildings using shear-bending model and ARX model: Experimental investigation", *Earthq. Struct*., **8**(4), 843-857.

Ghanem, R. and Shinozuka, M. (1995), "Structural-system identification I: Theory", *J. Eng. Mech*., ASCE, **121**(2), 255-264.

Hart, G.C. and Yao, J.T.P. (1977), "System identification in structural dynamics", *J. Eng. Mech. Div.*, ASCE, **103**(EM6), 1089-1104.

Hernandez-Garcia, M.R., Masri, S.F., Ghanem, R., Figueiredo, E. and Farrar, C.R. (2010), "An experimental investigation of change detection in uncertain chain-like systems", *J. Sound Vib*., **329**(12), 2395-2409.

Hjelmstad, K.D., Banan, M.R. and Banan, M.R. (1995), "On building finite element models of structures from modal response", *Earthq. Eng. Struct. Dyn.*, **24**, 53-67.

Housner, G.W. *et al*. (1997), "Structural control: past, present, and future", *J. Engng. Mech.*, ASCE, **123**(9), 897-971.

Ikeda, A., Minami, Y., Fujita, K. and Takewaki, I. (2014a), "Smart system identification of super high-rise buildings using limited vibration data during the 2011 Tohoku earthquake", *Int. J. High-Rise Build.*, **3**(4), 255-271.

Ikeda, A., Fujita, K. and Takewaki, I. (2014b), "Story-wise system identification of shear building using ambient vibration data and ARX model", *Earthq. Struct.*, **7**(6), 1093-1118.

Inaudi, J.A and Kelly, J.M. (1995), "Linear hysteretic damping and the Hilbert transform", *J. Eng. Mech.*, ASCE, **121**(5), 626-632.

Ji, X., Fenves, G.L., Kajiwara, K. and Nakashima, M. (2011), "Seismic damage detection of a full-scale shaking table test structure", *J. Struct. Eng.*, ASCE, **137**(1), 14-21.

Johnson, E. and Wojtkiewicz, S. (2014), "Efficient sensitivity analysis of structures with local modifications. II: Transfer functions and spectral densities", *J. Eng. Mech.*, ASCE, **140**(9), 04014068.

Kuwabara, M., Yoshitomi, S. and Takewaki, I. (2013), "A new approach to system identification and damage detection of high-rise buildings", *Struct. Control Hlth. Monit.*, **20**(5), 703-727.

Lus, H., Betti, R., Yu, J. and De Angelis, M. (2004), "Investigation of a system identification methodology in the context of the ASCE benchmark problem", *J. Eng. Mech.*, ASCE, **130**(1), 71-84.

Masri, S.F., Nakamura, M., Chassiakos, A.G. and Caughey, T.K. (1996), "A neural network approach to the detection of changes in structural parameters", *J. Eng. Mech.*, ASCE, **122**(4), 350-360.

Mei, Q. and GülNovel, M. (2014), "Sensor clustering-based approach for simultaneous detection of stiffness and mass changes using output-only data", *J. Struct. Eng.*, ASCE, **140**(10), 04014237.

Minami, Y., Yoshitomi, S. and Takewaki, I. (2013), "System identification of super high-rise buildings using limited vibration data during the 2011 Tohoku (Japan) earthquake", *Struct. Control Hlth. Monit.*, **20**(11), 1317-1338.

Nagarajaiah, S. and Basu, B. (2009), "Output only modal identification and structural damage detection using time frequency & wavelet techniques", *Earthq. Eng. Eng. Vib.*, **8**(4), 583-605.

Nashif, A.D., Jones, D.I.G. and Henderson, J.P. (1985), *Vibration Damping*, John Wiley & Sons.

Safak, E. (1989), "Adaptive modeling, identification, and control of dynamic structural systems. I: Theory", *J. Eng. Mech.*, ASCE, **115**(11), 2386-2405.

Takewaki, I. and Nakamura, M. (2000), "Stiffness-damping simultaneous identification using limited earthquake records", *Earthq. Eng. Struct. Dyn.*, **29**(8), 1219-1238.

Takewaki, I. and Nakamura, M. (2005), "Stiffness-damping simultaneous identification under limited observation", *J. Eng. Mech.*, ASCE, **131**(10), 1027-1035.

Takewaki, I. and Nakamura, M. (2009), "Temporal variation of modal properties of a base-isolated building during an earthquake", *J. Zhejiang University-Sci. A*, **11**(1), 1-8.

Takewaki, I., Nakamura, M. and Yoshitomi, S. (2011), *System Identification for Structural Health Monitoring*, WIT Press, UK.

Udwadia, F., Sharma, D. and Shah, C. (1978), "Uniqueness of damping and stiffness distributions in the identification of soil and structural systems", *J. Appl. Mech.*, ASME, **45**, 181-187.

Yao, J.T.P. and Natke, H.G. (1994), "Damage detection and reliability evaluation of existing structures", *Struct. Saf.*, **15**, 3-16.

Zhang, D. and Johnson, E. (2012), "Substructure identification for shear structures: cross power spectral density method", *Smart Mater. Struct.*, **21**(5), 055006.

Zhang, D. and Johnson, E. (2013a), "Substructure identification for shear structures I: Substructure identification method", *Struct. Control Hlth. Monit.*, **20**(5), 804-820.

Zhang, D. and Johnson, E. (2013b), "Substructure identification for shear structures with nonstationary structural responses", *J. Eng. Mech.*, ASCE, **139**(12), 1769-1779.

CC